Published in "Langmuir 29(29): 9188–9198, 2013"
which should be cited to refer to this work.

Host–Guest Interactions and Orientation of Dyes in the One-Dimensional Channels of Zeolite L

Ettore Fois,*[,†] Gloria Tabacchi,[†] André Devaux,[‡] Peter Belser,[‡] Dominik Brühwiler,[§] and Gion Calzaferri[∥]

[†]Department of Science and High Technology, University of Insubria, and INSTM, Via Lucini 3, I-22100 Como, Italy
[‡]Department of Chemistry, University of Fribourg, Chemin du Musée 9, CH-1700 Fribourg, Switzerland
[§]Institute of Chemistry and Biological Chemistry, Zurich University of Applied Sciences, CH-8820 Wädenswil, Switzerland
[∥]Department of Chemistry and Biochemistry, University of Bern, Freiestrasse 3, CH-3012 Bern, Switzerland

ABSTRACT: A combined experimental and modeling study of methylacridine ($MeAcr^+$) dye-zeolite L composites unravels the microscopic origin of their functional properties. The anisotropic orientation of the cationic dye inside the ZL channel is unambiguously determined and understood. The most stable orientation of $MeAcr^+$, which features both its long and short molecular axes nearly perpendicular to the channel axis, is mainly determined by dye-ZL electrostatic interactions but also depends on the cosolvent water. In ZL, $MeAcr^+$ is not hydrogen bonded to water or ZL framework oxygens and is hydrophobically solvated by water molecules. These findings further support the hypothesis that the cosolvent can importantly influence properties of dye–zeolite composites. Of relevance for a deeper comprehension of the physical chemistry of these hybrids is the observation that trivial energy transfer processes (self-absorption) are often playing a significant role in the optical properties of the composites.

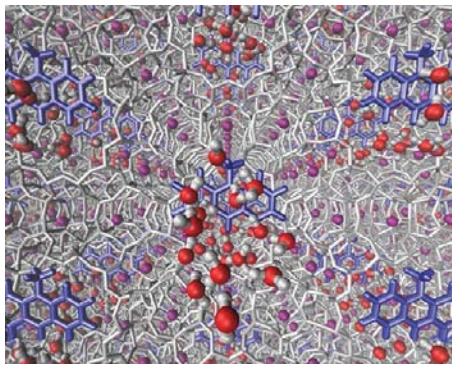

1. INTRODUCTION

Utilization of the one-dimensional channel framework of zeolite L (ZL) as a host for molecules and complexes has led to organized objects with a wide range of properties.[1−4] The narrow channels can prevent sufficiently bulky molecules from passing each other, allowing the realization of well-defined domains inside of the channels. Guests can be chosen in such a way that they can stack inside, forming, e.g., H-type aggregates,[5] or that they can at best touch each other at van der Waals distance, leading, e.g., to J-aggregate coupling,[6] or that any intermolecular interaction becomes negligibly small. This means that guest–guest interactions can be fully controlled by means of molecular engineering. ZL crystals can be synthesized in a wide size range, from about 30 nm up to at least 10 000 nm, with disc, barrel, or elongated morphology.[7−10] The channel openings of guest–ZL composites can be either modified with functional stopcock molecules or fully sealed in order to inhibit any matter exchange with the environment.[1,6] The cation-exchange properties allow using the ship-in-a-bottle synthesis procedure[11] to form thermally stable rare-earth complexes.[12] These ZL features are extremely useful in synthesizing objects that open new perspectives in areas of topic relevance, ranging from light harvesting, over information processing, to analytical and biomedical tools. The anisotropic arrangement of dye molecules, which can result in efficient electronic excitation energy migration, mimicking the operating properties of photosynthetic organisms,[1,6,13] is the basis of the functionality of ZL devices.

Early studies on dye-zeolite composites were performed preferentially using zeolite Y and $AlPO_4$-5 as hosts.[11,14−16] Important observations regarding the influence of the cosolvent and the cocations in zeolite Y have been made by V. Ramamurthy and reviewed in ref 14. Also, the properties of hierarchically organized luminescent hybrid materials have been recently reviewed in refs 1 and 17. Electronic transition properties have been studied by luminescence and diffuse reflectance spectroscopy; results of the latter are, however, often unsatisfactory and difficult to interpret. In many cases very good electronic transmission spectra can be obtained by dispersing the dye-zeolite crystals in an appropriate solvent that acts as a refractive index matching medium; moreover, surface modifications of the crystals and especially embedding in a polymer matrix allow for measuring good electronic transmission spectra and are well suited for quantitative measurements on oriented monolayers.[13,18] Recently we developed the very useful and convenient oil-glass-sandwich (OGS) sample preparation method, which is also used in the present study.[19]

Supramolecular organization inside the ZL nanochannels depends on the dyes' orientation, which is affected by geometric constraints (channel diameter, size, shape, and charge of the guests), cocations, and cosolvent molecules. Qualitative knowledge of these features is, in general, not

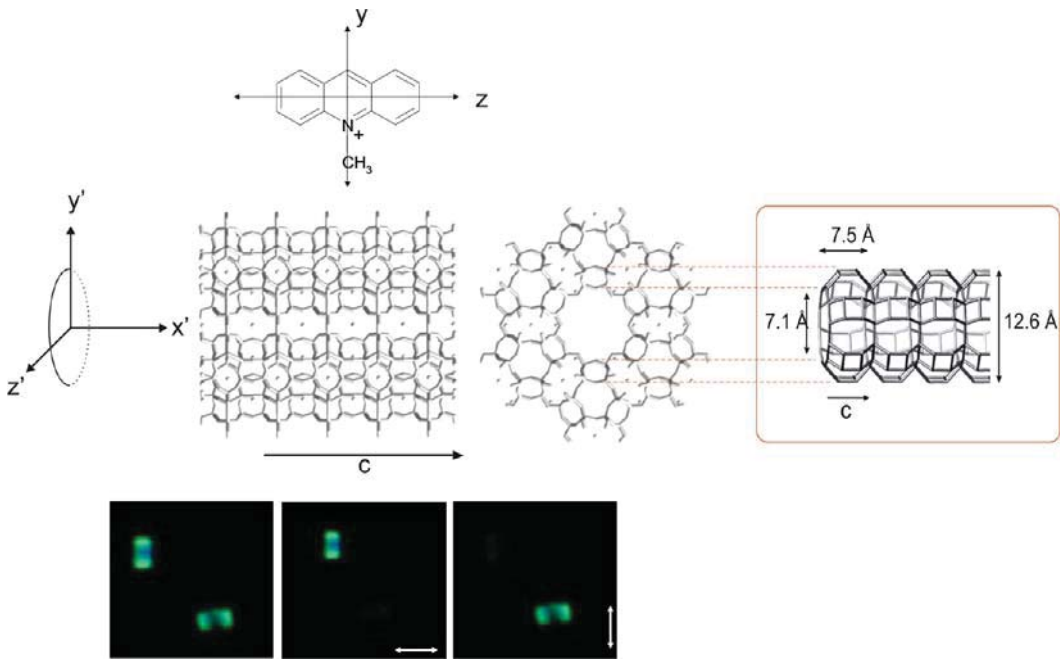

Figure 1. Top: Structure of $MeAcr^+$ and coordinate system. Middle: Side and top view of a ZL channel, with coordinate system. The *c* axis coincides with the channel axis. The length of the unit cell is 7.5 Å; 7.1 Å is the smallest and 12.6 Å is the largest channel diameter. Bottom: Fluorescence microscopy images of two $MeAcr^+$-ZL crystals with a length of about 2 μm: left, observed without a polarizer; middle and right observed through a polarizer, the orientation of which is indicated by the double arrow.[18]

sufficient for determining and understanding the distribution of dye orientations. Good information can be obtained experimentally through optical spectroscopy of oriented dye−ZL monolayers[13,18] or by advanced fluorescence microscopy techniques,[20−22] which are related to the orientation of the electronic transition dipole moment (ETDM) of the molecules with respect to the ZL channel axis. Interpretation is, however, not always unambiguous because even single crystal microscopy data are the result of averaging over a large number of situations. Moreover, in spite of quantum chemistry's long tradition in zeolite science,[23,24] the modeling of dye−ZL composites remains challenging because of the considerable size of the systems to be handled in the calculations.

The orientation of xanthene dyes inside ZL nanochannels has been an enigma for many years because the angle formed by the dyes ETDM with the channel axis, deduced from fluorescence microscopy experiments, was incompatible with the relative dimensions of the molecule and the nanochannel.[21,22] Theoretical modeling of the oxonine−ZL composite solved the issue recently by unraveling the orientation of the dye and revealing that it was determined by water.[25] This result was surprising because in the case of another dye, fluorenone, orientation was determined by the interaction between fluorenone carbonyl oxygen and the ZL extraframework potassium cations.[26,27]

The finding that hydration and dehydration can change the preferential orientation of the photoactive species may be of key relevance for understanding and designing supramolecular organization in hybrid functional materials: for example, relevant properties of dye−zeolite based devices might be tuned by a proper choice of the cosolvent. In order to better understand the role of water, we extended the theoretical and experimental studies to the cationic dye methylacridine ($MeAcr^+$), which allows monitoring both the first and the second electronic transitions. $MeAcr^+$ is shorter than the dyes oxonine and pyronine, small enough to fit into one unit cell of ZL, has no NH_2 groups at both ends, and charge is located in the middle of the molecule; see Figure 1.

Both $MeAcr^+$ and $HAcr^+$ have been inserted into the channels of ZL,[3,18] and their electronic absorption spectra have been studied experimentally in much detail, revealing that the relatively weak S_0-S_1 transition is oriented parallel to the *y* axis (^1L_a), while the more intense S_0-S_2 is parallel to z (^1L_b) (see Scheme 1). Both transitions are of $\pi-\pi^*$ type;[28,29] the symbols ^1L_a and ^1L_b refer to Platt's nomenclature for cata-condensed hydrocarbons.[30] $MeAcr^+$ was chosen because single crystal fluorescence microscopy observations allowed us to monitor the orientation of the S_0-S_1 transition and polarized electronic absorption spectra of the S_0-S_2 band have also been measured on oriented $MeAcr^+$-ZL monolayers.[18] While the orientation of the S_0-S_1 ETDM could be relatively well assigned, significant uncertainty remained for the S_0-S_2 ETDM, and it was not possible to deduce the orientation of the molecule with respect to the ZL channel axis in a satisfactory manner.

Deep insight into the exact orientation of the dye and the influence of the cosolvent water was obtained by modeling the behavior of $MeAcr^+$ in ZL, both under dry and wet conditions, and by comparing the electronic absorption and fluorescence spectra of aqueous solutions of $MeAcr^+$ with those of $MeAcr^+$−ZL composites.

2. RESULTS AND DISCUSSION

Before presenting our results, it should be recalled that ZL allows, through geometrical constraints, the realization of extremely high concentrations of well-oriented molecules; as an example, a 60 nm by 60 nm ZL crystal can host up to nearly 40000 guests that occupy 2 unit cells. It is convenient to use the occupation probability *p* as parameter, see eq 1, to express the dye concentration based on geometrical (space-filling) proper-

Scheme 1. Definition of the Orientation of the S_0-S_1 (^1L_a) and S_0-S_2 (^1L_b) ETDM As Well As of the Angles η and θ Used to Describe the Orientation of $MeAcr^+$ Inside of the ZL Channels[a]

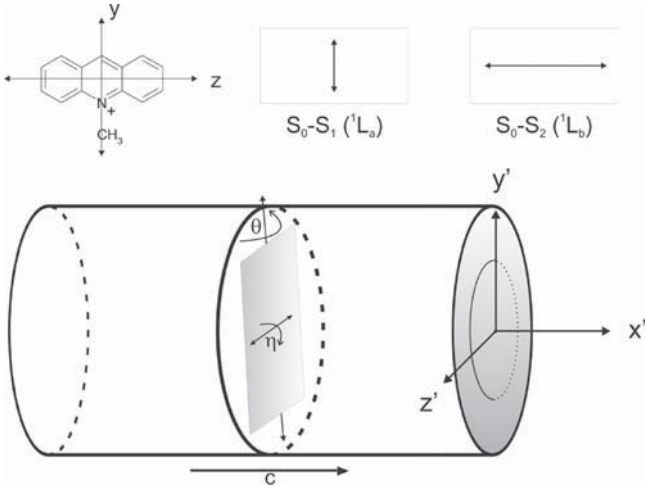

[a]Upper: $MeAcr^+$ is sketched as rectangle and the orientations of the ETDMs as double arrows. Lower: the drawing shows the position of $MeAcr^+$ in the (y',z') plane which corresponds to the angles $(\eta,\theta) = (90°,90°)$.

ties of the host, i.e., showing to what extent the ZL channels are filled with dye molecules.

$$p = \frac{\text{number of occupied sites}}{\text{total amount of sites}} \quad (1)$$

The loading p ranges from 0 for an empty ZL to 1 for a fully loaded one. The dye concentration $c(p)$ in a guest-ZL composite can be expressed as a function of the occupation probability, as described by eq 2:

$$c(p) = 0.752\frac{p}{n_s}\left(\frac{\text{mol}}{\text{L}}\right) \quad (2)$$

The symbol n_s represents the number of unit cells occupied by a guest. It can, for example, be equal to 1, 2, or 3, but n_s is not necessarily an integer. It is reasonable to set n_s for molecules of the size of $MeAcr^+$ or $HAcr^+$ to 1. This means, e.g., that $p = 0.1$ corresponds to a local dye concentration in the composite of 0.0752 mol/L. Both dyes can be inserted into the channels of ZL, thus forming $MeAcr^+$−ZL and $HAcr^+$−ZL guest−host composites that exhibit pronounced anisotropic optical properties.[3,18]

2.1. Electronic Absorption and Fluorescence Spectra. The absorption and fluorescence spectra of $MeAcr^+$ in aqueous solution and embedded in ZL, recorded at ambient conditions, are shown in Figure 2, while the band positions and their shifts are collected in Table S1. The $MeAcr^+$−ZL spectra were measured by using the OGS sample preparation technique that allows for a sufficient suppression of the light scattering due to the ZL host. The fluorescence spectra shown were measured upon excitation close to the maximum of the more intense S_0-S_2 band at 355 nm, and were observed to be identical when excited close to the maximum of the less intense S_0-S_1 band at 410 nm. The absorption spectrum of a 2.8×10^{-7} M solution is identical with the one shown in Figure 2, where the concentration was 2.8×10^{-6} M. The extinction coefficient at the maximum of the S_0-S_2 transition at 357 nm was

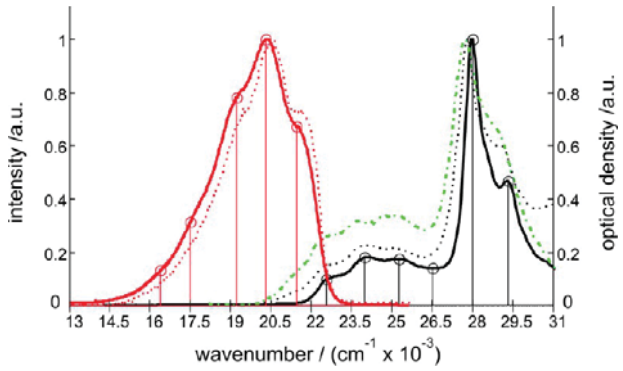

Figure 2. Absorption (black), fluorescence (red), and excitation (green) spectra. The solid lines show the absorption and the fluorescence spectra of a 2.8×10^{-6} M $MeAcr^+$ solution in water. The absorption and fluorescence spectra of a $MeAcr^+$−ZL composite with a loading $p = 0.01$ are dotted and the excitation spectrum of the same sample (observed at 560 nm) is dash-dotted.

determined as 21400 M^{-1} cm^{-1} while the coefficient corresponding to the S_0-S_1 transition at 415 nm is 4000 M^{-1} cm^{-1}. The presence of characteristic vibrational features in these spectra is remarkable: they differ little from those seen in the $MeAcr^+$−ZL composite and are equally present in the excitation spectrum. Since the shifts in peak position between the spectra in these environments are very small, the vibrational progression positions can be extracted, as indicated by means of vertical lines in Figure 2, for the aqueous solution spectra. The vibrational energies in Table S1 are all in the same range of about 1200 cm^{-1} and are probably related to aromatic C−H bending and/or C−C stretching vibrations.

The intensity of the S_0-S_1 transition seen in the excitation spectrum is larger than observed in the absorption spectra because the fluorescence yield upon excitation into the S_1 state is larger than upon excitation of the S_2 state. From the nearly perfect mirror symmetry between the $S_0 \rightarrow S_1$ absorption and the $S_0 \leftarrow S_1$ fluorescence bands, as well as from the fact that the vibrational features are well developed with similar band shifts, we conclude that there is very little difference between the potentials of the S_0, S_1, and S_2 states. We can also conclude that the minimum positions of the S_0 and the S_2 potentials are about identical while that of the S_1 is slightly displaced with respect to the previous two. Altogether, these observations suggest that the $MeAcr^+$ structure and solvation environment in the S_2 and S_1 states should be quite close to the ground state ones. The value of the oscillator strength for the S_0-S_1 and the S_0-S_2 transitions can be deduced from the absorption spectrum in water to be about 0.023 and 0.19, respectively. A change in the intensity ratio between the $S_0 \rightarrow S_1$ and $S_0 \rightarrow S_2$ bands in passing from the isotropic liquid medium to the zeolite is also observed.

The polarization of the S_0-S_1 (^1L_a) and of the more intense S_0-S_2 (^1L_b) transitions of $MeAcr^+$ in $MeAcr^+$−ZL composite crystals are discussed in Figure 1 and Scheme 1, where the hexagonal ZL crystals are sketched as cylinders in order to better outline the essentials of the anisotropy. The S_0-S_1 (^1L_a) transition is oriented perpendicular to the c axis of the crystal, as seen in the fluorescence microscope image in Figure 1. The orientation of the S_0-S_2 (^1L_b) transition has been studied by absorption spectroscopy of an oriented $MeAcr^+$−ZL monolayer on a quartz plate, as depicted in Figure 3.[18] From this we have concluded, however with much uncertainty, that the observed

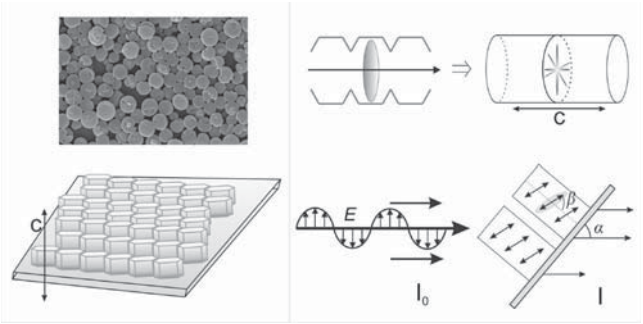

Figure 3. Depiction of the polarized electronic absorption spectra measurements on oriented dye−ZL monolayers reported in refs 13 and 18. Left. SEM image of a ZL monolayer on glass. Length and diameter of the crystals shown is about 1 μm. The scheme below explains the orientation of the crystals c axis with respect to the surface. Right. Scheme of a ZL channel containing a $MeAcr^+$ dye lying in the (y',z') plane defined in Figure 1. The angle α describes the orientation of the layer, symbolized by two crystals, with respect to the incoming light with intensity I_0 before and I after passing the layer. The angle β describes the orientation of the ETDM probed by the incoming light.

anisotropy is compatible with the assumption that angle θ (Scheme 1) describing the orientation of the S_0−S_2 ETDM is probably large.[18]

The local concentration of molecules in dye-ZL composites as monomers can be very high, see eq 2, especially compared to homogeneous solutions where solubility and aggregation prevent reaching similar values. As a consequence, self-absorption, sometimes also called trivial energy transfer process,[31] can occur within individual dye−ZL crystals, depending on the crystal size or the thickness of the measured layer, and is negligible only at low loading. This phenomenon and its effect on the emission band shapes have been discussed in previous publications.[13] Self-absorption causes an apparent bathochromic shift of the fluorescence spectrum and a corresponding distortion. It can be reasonably well simulated without much effort in a simple model.[32] A quantitative reproduction can be difficult because complicated geometrical aspects, including light scattering, have to be considered.[33,34] Understanding the consequences of self-absorption is important in order to avoid drawing wrong conclusions. We therefore illustrate in Figure 4 the effect of self-absorption for $MeAcr^+$−ZL composites on the measured fluorescence spectra at three different loadings. The right part of this Figure illustrates the results obtained by the simulation. The simple simulation reproduces the main features of the changes caused by self-absorption sufficiently well for our purpose.

2.2. Computational Results. Experimental results on $MeAcr^+$ in water and ZL leave some open questions on the dye orientation and on the possible origin of the close similarity of $MeAcr^+$ electronic spectra in these different environments. We have addressed these questions by first principles modeling. As a first step, the electronic excitation energies and the ETDM of the isolated $MeAcr^+$ molecule have been calculated at the EOM-CCSD[35] and TD-cam-b3lyp[36,37] levels and summarized in Table 1. Overall, the agreement among electronic properties calculated by the two approaches is satisfactory ($\Delta\lambda \approx 11$ nm for the $S_0 \rightarrow S_1$ vertical transition); electronic excitation wavelengths calculated for isolated $MeAcr^+$ are blue-shifted with respect to the experimental values for $MeAcr^+$ in water and in ZL.

The first electronic excitation, $S_0 \rightarrow S_1$, corresponds to the HOMO−LUMO ($\pi \rightarrow \pi^*$) transition, while the $S_0 \rightarrow S_2$ one involves an admixture of $(\pi - 1) \rightarrow \pi^*$ and $\pi \rightarrow (\pi + 1)^*$ transitions.

The $S_0 \rightarrow S_1$ and $S_0 \rightarrow S_2$ ETDM are aligned along the short and the long molecular axis, respectively (see Figure 1 and Scheme 1), in full agreement with the dichroic measurements of $MeAcr^+$ embedded in stretched polyvinyl alcohol films.[28,29] Moreover, the $S_0 \rightarrow S_1$ and $S_0 \leftarrow S_1$ ETDMs are nearly parallel, indicating that absorption and emission optical data provide identical information on the dye orientation. A red shift of ~3700 cm^{-1} is predicted for the $S_0 \leftarrow S_1$ transition relative to the $S_0 \rightarrow S_1$ one. Remarkably, the vibrational pattern calculated for the S_0 state (not shown) presents an intense A′ mode at about 1300 cm^{-1} which involves a symmetric breathing of the $MeAcr^+$ aromatic rings (see Figure S1 in the Supporting Information). On this basis, we propose that the well developed vibrational pattern of Figure 2 is due to this A′ mode.

While calculations on isolated $MeAcr^+$ allow identifying the molecular mode detected in the experimental electronic spectra, theoretical results on the $MeAcr^+$−ZL composite, modeled at dry and wet conditions, reveal the preferential orientation of $MeAcr^+$ in the ZL nanochannels, highlighting an interesting solvation effect.

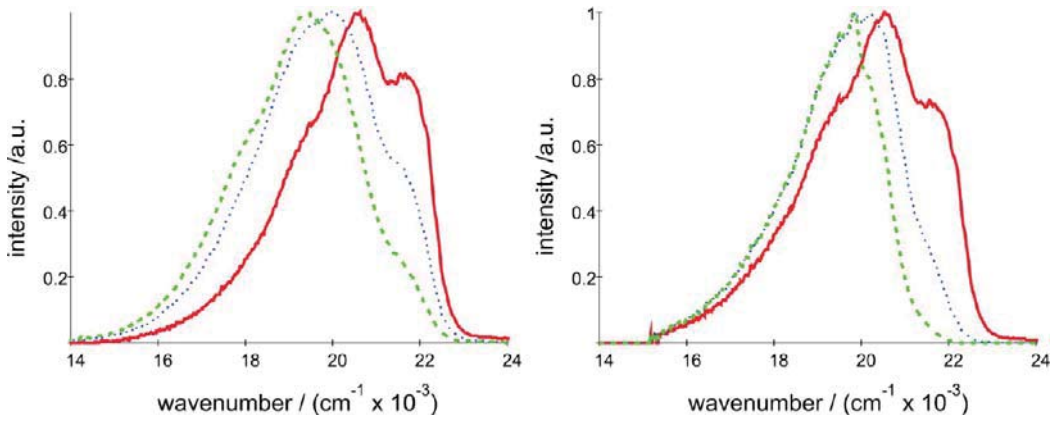

Figure 4. Self-absorption. Left: experimental fluorescence spectra measured for three samples with different loading. All spectra were scaled to 1 at their respective maxima. Red, solid: $p = 0.01$; blue, dotted $p = 0.06$; green, dashed $p = 0.15$. Right: calculated fluorescence spectra for the same loadings, by taking self-absorption into account.

Table 1. Calculated Electronic Excitation Properties[a]

(A) EOM-CCSD				
transition	λ [nm]	wavenumbers [cm^{-1}]	ETDM [a.u.]	f
6-311++g(2df,pd)				
$S_0 \rightarrow S_1$ A′, (^1L_a)	358.1	27922.0	(0.0108, 0.9029, 0.0)	0.0768
$S_0 \rightarrow S_2$ A″, (^1L_b)	318.4	31412.0	(0.0, 0.0, 1.2999)	0.1811
aug-cc-pvdz				
$S_0 \rightarrow S_1$ A′, (^1L_a)	357.5	27975.2	(0.0117, 0.8934, 0.0)	0.0755
$S_0 \rightarrow S_2$ A″, (^1L_b)	318.1	31435.7	(0.0, 0.0, 1.2806)	0.1787
D95V+(d)				
$S_0 \rightarrow S_1$ A′, (^1L_a)	350.7	28513.6	(0.0107, 0.9367, 0.0)	0.0850
$S_0 \rightarrow S_2$ A″, (^1L_b)	314.9	31758.1	(0.0, 0.0, 1.2655)	0.1768
(B) TD-cam-b3lyp				
transition	λ [nm]	wavenumbers [cm^{-1}]	ETDM [a.u.]	f
$S_0 \rightarrow S_1$ A′, (^1L_a)	369.2	27081.9	(0.0117, 0.8809, 0.0)	0.0638
$S_0 \rightarrow S_2$ A″, (^1L_b)	307.5	32521.4	(0.0, 0.0, 1.5869)	0.2488
$S_0 \leftarrow S_1$ A′, (^1L_a)	428.9	23316.0	(0.0195, 0.9358, 0.0)	0.0621

[a]The entries refer to excitation wavelength, excitation energy, (x,y,z) components of the ETDM, and oscillator strength f. (A) Electronic excitation properties calculated, on a MP2/cc-pvtz optimized $MeAcr^+$ isolated structure, at the EOM-CCSD level of theory with different basis sets. (B) Electronic excitation properties calculated at the TD-cam-b3lyp/6-311++(2df,dp) theory level. The $S_0 \leftarrow S_1$ transition properties were obtained by adopting the optimized S_1 geometry.

The η and θ angles (Scheme 1) calculated for the optimized structures of the $MeAcr^+$−ZL models, as well as the relative stability of the energy minima for both dry and wet conditions are collected in Table 2. The data clearly evidence that different orientations of the dye are possible; however, some orientations are energetically favored. At both dry and hydrated conditions, $MeAcr^+$ is preferentially perpendicular to the channel axis but can be found also nearly parallel to the channel or with a tilted orientation, even though at higher energies. These less stable arrangements are very important because they ensure the mobility of the dye along the channel (see below). The most stable structures are characterized by large η and θ values, close to 90°, in agreement with experimental observations, and are considerably lower in energy with respect to structures with the nearly parallel S_0−S_1 ETDM orientation. Indeed, the energy minimum at dry conditions Opt1 (see Table 2) is 25.0 kcal/mol more stable than the structure with θ = 10.8°. Interestingly, the energy difference between the minimum (η = 76.7°) and the structure with the lowest η value (η = 10.8°) increases to 51.6 kcal/mol in the presence of water, indicating a significant effect of the solvent on both the S_0−S_1 and the S_0−S_2 ETDM orientations, which motivates the dye to position itself into the (y',z') plane (Scheme 1). Such an effect is evidenced by Figure 5, representing the superposition of the minimum energy

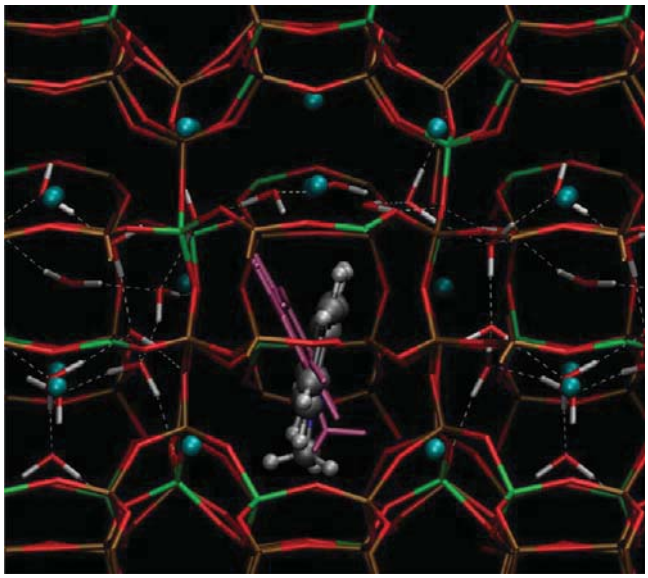

Figure 5. Superposition of the minimum energy structures of the $MeAcr^+$−ZL·$18H_2O$ composite (with $MeAcr^+$ in ball-and-stick representation: C, gray; N, blue; H, white) and of dry $MeAcr^+$−ZL (with $MeAcr^+$ in pink, stick representation). Color codes: Si, brown; O, red; Al, green; K, cyan; H, white. The dashed lines represent hydrogen bonds.

structures of the $MeAcr^+$−ZL composite at dry and wet conditions; in particular, hydration shifts the S_0-S_1 ETDM toward larger η values, i.e, nearly perpendicular to the channel axis.

The minimum energy structure of the hydrated composite is characterized by 6-membered "rings" of water molecules interacting with the ZL channel walls and the K^+ extra framework cations; the dye, however, does not form hydrogen bonds with the water molecules or the ZL framework oxygens, as indicated by the corresponding pair distribution functions

Table 2. Optimized Structures for Dry $MeAcr^+$−ZL (left) and for Hydrated $MeAcr^+$−ZL·$18H_2O$ (Right) with Different Orientations η and θ

$MeAcr^+$−ZL				$MeAcr^+$−ZL·$18H_2O$			
system	η [°]	θ [°]	ΔE [kcal/mol]	system	η [°]	θ [°]	ΔE [kcal/mol]
Opt1	65.6	89.5	0	Opt1	76.7	89.9	0
Opt2	64.3	88.9	4.8	Opt2	79.1	42.4	2.5
Opt3	77.5	44.9	9.4	Opt3	63.5	89.8	2.7
Opt4	88.6	26.9	14.6	Opt4	41.6	88.1	9.5
Opt5	31.3	87.8	18.9	Opt5	86.2	8.1	23.7
Opt6	15.3	89.1	21.0	Opt6	10.8	88.3	51.6
Opt7	9.7	89.5	21.2				
Opt8	79.6	10.8	25.0				

(see Figure S3). Therefore, $MeAcr^+$ orientation inside ZL is mainly governed by electrostatic interactions, as demonstrated by the electrostatic potential maps reported, for selected optimized structures, in Figure 6. It emerges that energetically

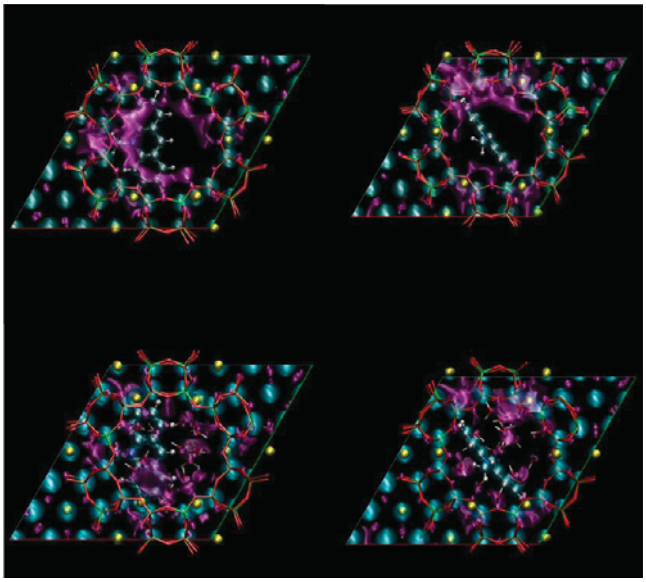

Figure 6. Electrostatic potential contour maps for selected optimized geometries of the ZL/$MeAcr^+$ composite. Top: dry Opt1 (left) and dry Opt8 (right) systems. Bottom: hydrated Opt1 (left) and hydrated Opt6 (right) systems. Atoms color codes: Si, brown; O, red; Al, green; K, yellow; C, gray; N, blue; H, white. Negative electrostatic potential surfaces in purple, positive ones in cyan.

favored structures correspond to orientations where the $MeAcr^+$ $(N-CH_3)^+$ group is in close contact with negatively charged regions of the zeolite host.

On this basis, it is now possible to understand why structures characterized by a nearly perpendicular orientation of both the short and the long $MeAcr^+$ axis with respect to the ZL channel axis are energetically favored. Such an orientation ensures the most favorable Coulomb interaction because the $MeAcr^+$ methyl group points toward the most negatively charged region of the ZL framework, which features three Al atoms at 4.1–4.2 Å distance from the $MeAcr^+$ methyl-carbon. On the contrary, in the less stable structure at wet conditions (Opt6, η = 10.8°, ΔE = 51.6 kcal/mol), the $MeAcr^+$ methyl group points toward the center of the channel and the minimum distance between the methyl group and the Al framework atoms is well above 5 Å, as indicated by the corresponding radial distribution function $g(r)$, shown in Figure 7 (top). Similar results were obtained for the dry systems (see Figure S2).

These findings are corroborated by the FPMD results on the hydrated composite, at room temperature conditions. Three simulations have been performed: MD1, started from the minimum energy structure Opt1, where the $MeAcr^+$ long axis is perpendicular to the channel, MD5, started from Opt5, where the long axis is parallel, and MD6, started from Opt6, where the short axis is parallel. Remarkably, in all simulations the dye keeps, on average, its initial orientation, showing only small oscillations with respect to the starting configuration: the average orientation angle θ calculated for the simulations amounts to 87.5°, 5.6°, and 87.3° for MD1, MD5, and MD6, respectively (the corresponding standard deviations are 1.8°, 3.3°, and 1.6°). Neither translation along the channel nor

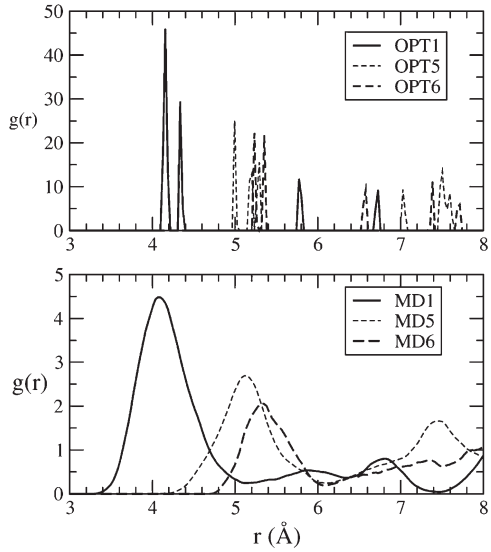

Figure 7. Top panel: radial distribution function $g(r)$ representing the (methyl-carbon)–Al distance for the minimum energy structure Opt1 (solid line) and for higher energy structures Opt5 (dotted line) and Opt6 (dashed line) of the $MeAcr^+$–ZL·$18H_2O$-composite. Bottom panel: radial distribution function g(r) for the FPMD simulation MD1 of the hydrated composite started from Opt1 (solid line), for the FPMD simulation of the hydrated composite started from Opt5 (MD5, dotted line), and for the MD6 trajectory, started from Opt6 (dashed lines).

significant reorientation of the dye have been detected, at the picoseconds time-scale accessible to FPMD, along these simulations. In contrast, FPMD simulations of the dry system, starting from the least stable structure Opt8, highlighted a significant mobility of $MeAcr^+$ along the ZL empty channel (see movie 1 in the SI). Such a different behavior is due to the hampering effect of the solvent, which, as evidenced by recent studies on dye–ZL composites,[25,26] influences the dynamic properties of the composite through strong water–water hydrogen bonds (see Figure S4). Actually, literature work on zeolitic water[38,39] indicates that the water–water hydrogen bonding network causes a slowing-down of the water orientational dynamics in zeolite nanochannels that, in turn, hampers the motion of the dye. Interestingly, in this case the slowing-down occurs even in the absence of hydrogen bonds between $MeAcr^+$ and water molecules (see Figure S3). However, temperature-induced fluctuations of the $MeAcr^+$ molecular geometry from planarity also occur, indicating a certain degree of flexibility of the dye structure. Such a feature, also detected in the case of other dye–ZL composites,[25,26] may play a key role in facilitating the diffusion of dye molecules through the ZL channels.[25]

Concerning the orientation of the $MeAcr^+$ ETDM at room temperature conditions, the average angle η resulting from the MD1, MD5, and MD6 trajectories is 72.2°, 86.7°, and 10.1°, respectively (the corresponding standard deviations are 7.9°, 2.8°, and 5.8°). In line with the results of the 0 K optimized structures, in MD1 the methyl group of the dye gets closer to the negatively charged regions of the ZL framework, as indicated by the radial distribution functions in Figure 7 (bottom). Therefore, room temperature simulations results confirm that the most favorable orientation of $MeAcr^+$ inside ZL is with both its long axis (S_0–S_2 ETDM) and its short axis (S_0–S_1 ETDM) nearly perpendicular to the ZL channel.

As in the case of oxonine– and pyronine–ZL composites,[25] the perpendicular arrangement implies dye confinement in a single ZL cell and allows the nearby cells to be fully occupied by water molecules as in pristine ZL structures. The H_2O arrangement in MeAcr$^+$–ZL·18H_2O (Opt1 structure), shown in Figure 8, evidences that water molecules are actually

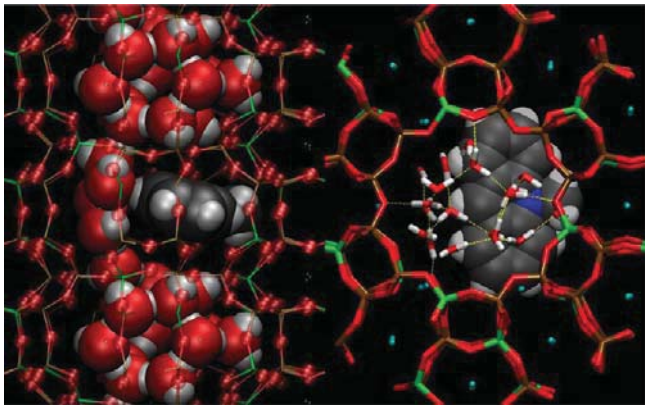

Figure 8. Representations of the Opt1 structure of the MeAcr$^+$–ZL·18H_2O composite. Left panel: projection in the (x',z') plane, Right panel: projection in the (y',z') plane. Atom color codes as in Figure 5. On the left panel, MeAcr$^+$ and water molecules are represented as van der Waals spheres, while framework oxygen atoms are represented as small spheres. On the right panel, MeAcr$^+$ is represented as van der Waals spheres.

"solvating" the cationic dye, even without being involved in dye-water hydrogen bonding (see Figure S3). Such a hydrophobic hydration shell is ultimately due to the MeAcr$^+$ structure, which has no sites capable of forming H-bonding. On the whole, these findings shed light on a new aspect of physicochemical interactions in composite materials: here, the leading host–guest interaction, which lie at the origin of the hybrid material functional properties, is electrostatics. Such a situation is different from that typical of many host–guest composites where hydrogen bonding usually plays a relevant role as, e.g., in coumarin derivatives incorporated in mesoporous silica,[40] in the Maya Blue pigment,[41,42] in composites based on DNA as organizing agent,[43] or in systems where urea-based hydrogen bonding acts as a structure-directing agent in orienting zeolite monolayers.[44]

By adopting either a polarizable continuum medium (PCM)[45] model or a cluster model, cut from the Opt1 structure, we have calculated the first two excitations at the TD-cam-b3lyp level of theory (Table 3). In all cases the transitions involve the same electronic states. A red shift of the excitations is calculated in passing from MeAcr$^+$ in vacuum to MeAcr$^+$ embedded either in a continuum solvent model or in the zeolite environment. The calculated oscillator strength values suggest that the intensity of the $S_0 \rightarrow S_1$ transition is enhanced in ZL, while a decrease in intensity is predicted for the $S_0 \rightarrow S_2$ one, with respect to the vacuum. Interestingly, a decrease of the $(S_0 \rightarrow S_2)/(S_0 \rightarrow S_1)$ intensity ratio is predicted in passing from the isotropic medium [MeAcr$^+$ (PCM)] to the crystalline zeolite phase [MeAcr$^+$ (ZL,ZL)], in line with the experimental observation (see Figure 2). By comparing the results of the [MeAcr$^+$(ZL,ZL)] cluster with the ones of [MeAcr$^+$(Vac/ZL)], which contains an undistorted dye molecule, it is possible to disentangle the ZL embedding effects from molecular deformation effects. The lower red-shift found for

Table 3. Electronic Excitation Properties for Optimized Isolated MeAcr$^+$ in Vacuum (Vac,Vac), for MeAcr$^+$ Optimized in PCM, for the Isolated Dye Taken from the Hydrated Opt1 Structure (ZL,Vac), for the Optimized Isolated Dye in Vacuum Embedded in a ZL Cluster Cut from Hydrated Opt1 (Vac,ZL), for a MeAcr$^+$-ZL Cluster Cut from the Hydrated Structure Opt1 (ZL,ZL)[a]

	λ ($S_0 \rightarrow S_1$)	λ ($S_0 \rightarrow S_2$)
[MeAcr$^+$ (Vac,Vac)]	369.2 (0.0638)	307.5 (0.2488)
[MeAcr$^+$ (PCM)]	372.4 (0.0868)	313.0 (0.3232)
[MeAcr$^+$ (ZL/Vac)]	384.7 (0.0637)	317.9 (0.2441)
[MeAcr$^+$ (Vac/ZL)]	376.6 (0.0821)	310.7 (0.1427)
[MeAcr$^+$ (ZL,ZL)]	386.1 (0.0828)	316.6 (0.1495)
Exp.	410	355

[a]The experimentally observed transition wavelengths for the MeAcr$^+$ composite are reported for comparison. Transition wavelengths are given in nm with the corresponding oscillator strength in parentheses.

[MeAcr$^+$(Vac/ZL)] indicates that the ZL embedding effects are less effective in red-shifting the excitations than the joint embedding-deformation effect present in the [MeAcr$^+$(ZL,ZL)] model or than the pure deformation effects present in [MeAcr$^+$(ZL,Vac)]. Remarkably, the ZL environment mostly affects the intensity of the transitions. In any case, embedding and structural effects do not alter the ETDM direction with respect to the vacuum, as shown in Figure 9, where the

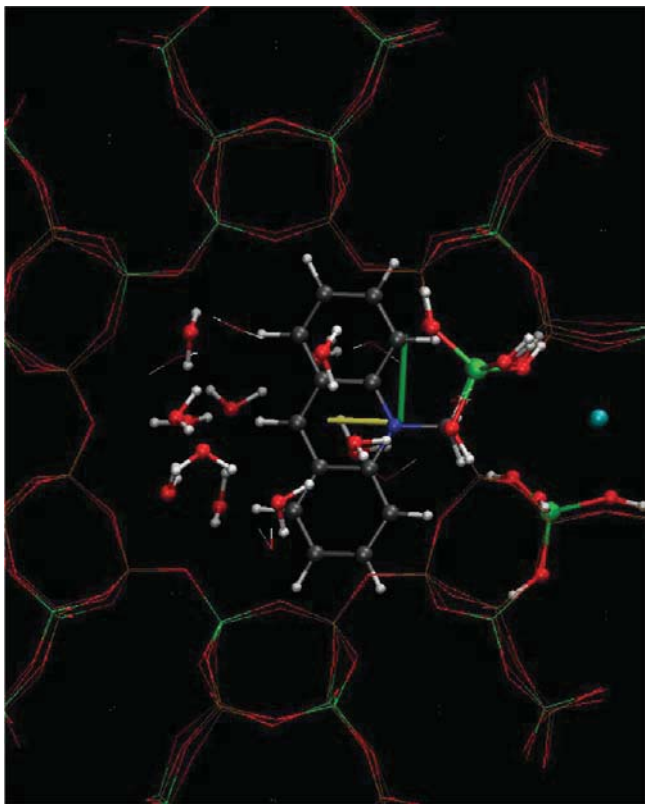

Figure 9. Graphical representation of the cluster model [MeAcr$^+$(ZL,ZL)] adopted for the electronic excitations calculation (atom color code as in Figure 5). The atoms included in the cluster are represented as ball-and-stick. The structure of the MeAcr$^+$–ZL·18H_2O composite (Opt1) is represented as thin lines. The ETDMs of the $S_0 \rightarrow S_1$ and $S_0 \rightarrow S_2$ transitions are represented as yellow and green thick lines, respectively.

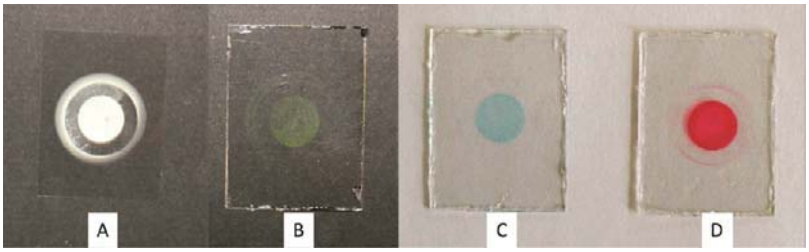

Figure 10. Photographic images of OGS. (A) Thin layer of $MeAcr^+$–ZL (p = 0.15) on a glass plate, as reference. (B) The same layer shown in (A) but after depositing a droplet of oil, covering with a glass plate and sealing. (C) and (D) The same as (B) but with different dyes. (C) terylene–ZL (p = 0.05); (D) terylene,perylene-ZL composite (p = 0.05, p = 0.5).

electronic transition dipoles calculated for the [$MeAcr^+$(ZL,ZL)] cluster are superimposed to the full periodic structure of the $MeAcr^+$-ZL·18H_2O-composite. The calculated ETDM angles η and θ for such a superposition amount to 78.1° and 90.7°, respectively, and are very similar to the values obtained from the geometrical parameters of the Opt1 structure (see Table 2).

3. CONCLUSIONS

The behavior of $MeAcr^+$–ZL composites has been studied via a combined experimental-modeling approach aimed at analyzing and understanding their peculiar optical properties. Reported data clearly indicate an anisotropic arrangement for the $MeAcr^+$ cationic dye inside the zeolite nanochannels, due to preferential orientation induced by (i) geometrical confinement in the one-dimensional channels; (ii) dye-dependent host–guest interactions; and (iii) cosolvent (water in this case) effects. Geometrical confinement induces a single-file arrangement of the dye in each zeolitic channel. The $MeAcr^+$ structure induces a preferential orientation of the molecules: the positively charged N–CH_3 groups point toward the negative-charge-bearing AlO_4 zeolite tetrahedra, and are positioned close to crystallographic sites normally occupied by K^+ cations. The cosolvent effects can be, in turn, split into two main contributions. The first pertains to water–water and water–zeolite interactions, that favor the clustering of water molecules via hydrogen bonding and induce the dye confinement into a single zeolite unit cell. The second cosolvent contribution is the hydrophobic solvation of the cationic dye, whose structure does not favor the formation of hydrogen bonds. The hydrophobic $MeAcr^+$ solvation, detected in hydrated ZL, raises an intriguing issue on the spectroscopic analyses of $MeAcr^+$, which reveal an impressive similarity of the dye electronic excitations/emissions energies and band shapes as measured in water solution and in the hydrated ZL composite. Indeed, even the vibronic features, remarkably detectable in both environments, are very similar. These close similarities suggest that hydrophobic solvation of $MeAcr^+$ might be operating in water as well.

Electronic excitation calculations, performed both for the isolated dye and for the dye surrounded by a cluster mimicking the hydrated zeolite environment, explain the microscopic origin of the excitation properties (i.e., energies, intensities and transition dipoles) and the effects of the environment on these properties. This insight, in combination with fluorescence microscopy data, allowed us to unambiguously determine the $MeAcr^+$ preferential orientation inside the zeolite channels. Self-absorption phenomena have been observed to be more important than what one might expect from a first glance of the spectral overlap region seen in Figure 2. This optical phenomenon is probably more common and easily underestimated in host–guest compounds which allow for a very large local concentration of well oriented dyes.

In more general terms, we have shown in this work how a multidisciplinary approach can be useful, and sometimes even necessary, to gather fundamental understanding of complex chemical systems. Such knowledge may be exploited in the development of devices based on dye–zeolite composites.

4. EXPERIMENTAL AND COMPUTATIONAL SECTION

4. 1. Experimental Procedures. *Materials.* Aluminum hydroxide, ABCR, dried gel, >99%; Aerosil OX-50, Degussa; potassium hydroxide, Fluka, purum p.a. >85%; methylacridine tetrafluoroborate, Aldrich; 1-butanol, Sigma-Aldrich, puriss p.a.; immersion oil, Sigma, for microscopy; base-coat nail varnish (Lady Manhattan Cosmetics, Pro Sine Base Coat). All materials were used as received without further purification.

Ion Exchange with Methylacridine Tetrafluoroborate. The dye methylacridine tetrafluoroborate (Aldrich Chemicals) was incorporated into ZL by means of an ion exchange process. Materials with three different loading degrees were prepared by suspending 30 mg of ZL in 0.36 mL (target p = 0.01), 3.6 mL (target p = 0.1), and 17.9 mL (target p = 0.5) of a 2.9 × 10^{-4} M aqueous dye solution. The solution was then left stirring at r t. for 24 h. The dye-loaded ZL was then centrifuged off at 2900 rpm for 15 min and washed two times with 20 mL portions of deionized water. The effective loading degrees were determined to be p = 0.01, p = 0.06, and p = 0.15, respectively (vide infra).

Determination of Loading Level by HF Analysis. The effective loading levels were determined by first suspending 2 mg of the loaded material in 3 mL ethanol (Honeywell, per analysis) in a PS cuvette. Six drops (300 μL) of a 4% aqueous HF solution were added to dissolve the zeolite. The process was completed after 30 min leaving a transparent solution. The loading degree was then calculated from the dye concentration obtained from the UV–vis absorption spectrum.

Preparation of Oil-Glass-Sandwiches for Spectroscopy. All absorption and luminescence spectra of dye-loaded ZL materials were recorded from oil-glass-sandwiches (OGS) prepared in a similar manner as reported in ref 19. The samples were prepared by suspending 1 mg of loaded material in 1 mL of 1-butanol (Sigma-Aldrich, puriss p.a.). A 200 μL droplet was then deposited on a glass microscopy coverslip (Marienfeld, 24 × 32 mm, No. 1). An aluminum ring with an inner radius of 15 mm confined the droplet's spread. Once the solvent was fully evaporated, the aluminum ring was removed and 300 μL of immersion oil (Sigma, for microscopy) was deposited on the thin ZL layer. Placing a second coverslip on top of the immersion oil and sealing the sides with base-coat nail varnish (Lady Manhattan Cosmetics, Pro Shine Base Coat) completed the sandwich. Examples of such an OGS are shown in Figure 10, which illustrates the disappearance of the strong light scattering of the unprotected layer (A) after completing the OGS (B). Important is the central part. The outer ring, which sometimes appears when the aluminum ring is not perfectly tight, can be avoided if necessary. The weak color of the $MeAcr^+$–ZL layer, not seen in (A), appears nicely in (B), and the sample is transparent in the visible region. We show in

(C) and (D) two clear dye−ZL composite layers to illustrate the usefulness of this simple technique.

4.2. Computational Models and Methods. *Isolated MeAcr$^+$.* Optimized geometries, vibrational frequencies, and electronic excitation properties of isolated MeAcr$^+$ were obtained adopting both wavefunction- and electron density-based approaches. The excitation properties of ground-state MeAcr$^+$ were obtained using the EOM-CCSD[35] method on the MeAcr$^+$ geometry optimized at the MP2/cc-pvtz level of theory. Geometry optimization was also performed by embedding MeAcr$^+$ in a polarizable continuum model of water (PCM)[45] at the MP2/cc-pvtz level.

Different basis sets were adopted for the electronic excitation, namely the D95V+(d), the aug-cc-pvdz and 6-311++g(2df,pd).[46] A density functional theory approach was used as well, by adopting the cam-b3lyp[36] approximation with the 6-311++g(2df,pd) basis set. With such approximation we have optimized MeAcr$^+$ in its S_0 state and, by using the TD approach,[37] in the first excited state S1. Harmonic frequencies for the S_0 ground state were calculated as well. The TD approach was used to calculate electronic transition properties. Calculations on isolated MeAcr$^+$ were performed with the g09 suite of programs.[47]

MeAcr$^+$−ZL System. Models of hydrated and dehydrated MeAcr$^+$−ZL composites were investigated by calculating both 0 K energy minima (geometry optimizations) and room temperature behavior (first principles molecular dynamics simulations) adopting the PBE approximation[48] to density functional theory (DFT) with a periodically repeated simulation cell. The all-potassium-form of ZL has been considered,[49] in line with the composition of the samples experimentally adopted.[18] The simulation cell consists of two ZL unit cells along c ($a = b = 18.466$ Å; $c = 2 \times 7.476$ Å; $\gamma = 120°$),[49] with a ZL framework formula of $[Al_{18}Si_{54}O_{144}]$. The simulation cell formula is $K_{17}[Al_{18}Si_{54}O_{144}]$MeAcr$^+$ because 18 positive charges per cell should balance the framework negative charge and MeAcr$^+$ is a cationic dye. The simulation cell stoichiometry of the dry model (MeAcr$^+$−ZL) was $K_{17}[Al_{18}Si_{54}O_{144}]$MeAcr$^+$.

MeAcr$^+$−ZL·18H$_2$O System. The simulation cell stoichiometry of the MeAcr$^+$−ZL·18H$_2$O hydrated model was $K_{17}[Al_{18}Si_{54}O_{144}]$-MeAcr$^+$·$(H_2O)_{18}$. The amount of water in the simulation cell was chosen on the basis of recent theoretical results[25] as well as on available literature data on ZL and ZL-based composites. All of the water molecules were placed inside the ZL channel. Guess positions were selected from the crystallographic water oxygen sites reported for pristine fully hydrated ZL,[50] by eliminating water molecules in close contact with MeAcr$^+$.

Both dry and hydrated MeAcr$^+$−ZL models contain 0.5 MeAcr$^+$ molecules per unit cell. As demonstrated and thoroughly discussed in ref 25, in such model system guest−guest interactions do not affect dye orientation at this loading.

Electron-ion cores interactions were treated with ultrasoft Vanderbilt pseudopotentials for H, C, and O; norm conserving pseudopotentials for Si, Al, and K (semicore).[51−54] Electronic orbitals were expanded in planewaves up to a 25 Ry cutoff (200 Ry for the density). Such a computational scheme for electronic structure treatment has been proved to properly describe large sized inorganic−organic systems including dye-zeolite hybrids.[25−27,55,56]

In the FPMD[57−59] simulations, a 0.121 fs time step and a 500 au electronic coefficients inertia parameter were used. After equilibration, trajectories were collected for ∼15 ps. Simulations were performed in the canonical ensemble (target temperature of the ionic thermostats: 300 K).[60]

Local energy minima were calculated by repeated simulated annealing/geometry optimization cycles on properly built guess configurations or on snapshots sampled from the FPMD simulations. In geometry optimizations, quasi-Newton methods were employed (convergence criterion: maximum force on nuclei of 1×10^{-4} hartree/bohr). In all optimizations and FPMD simulations, all atoms were allowed to move, no symmetry constraint (except from the box shape and size) was imposed, and periodic boundary conditions were applied.

A cluster cut from the optimized MeAcr$^+$−ZL·18H$_2$O geometry of the minimum energy structure Opt1 was adopted for the calculation of excitation properties, using the TD approach along with the cam-b3lyp functional with the g09 code.[47] In this case, the 6-311++g(2df,pd) basis set was adopted for the MeAcr$^+$ atoms, while the 6-31++g(d,p) basis set was adopted for the rest of the atoms in the cluster. The cluster model included the MeAcr$^+$ moiety, 12 water molecules, three Al$[OH]_4^-$ and two K$^+$ ions [MeAcr$^+$(ZL,ZL)]. The three AlO_4-tetrahedra and the two potassium cations closest to MeAcr$^+$ were included in the model cluster. The AlO_4-tetrahedra have been capped with H atoms that were positioned along the corresponding O−Si bonds at 1.0 Å from the oxygen atoms linked to Al. We have also calculated the electronic excitations on a cluster of the same size, [MeAcr$^+$(Vac,ZL)], in which the structure of the MeAcr$^+$ cation (as obtained from the Opt1 geometry) was replaced by the structure of MeAcr$^+$ optimized in vacuum. With such a stoichiometry, the model clusters are electrically neutral. We have also calculated the electronic excitation properties for the isolated cationic dye with the structure extracted from Opt1, [MeAcr$^+$(ZL,Vac)]. At this level of theory, the MeAcr$^+$ excitation properties were also calculated including the PCM model on the PCM optimized structure.

■ ASSOCIATED CONTENT

Supporting Information

Figure S1 describing the atomic displacements involved in the 1300 cm^{-1} A′ vibrational mode of MeAcr$^+$. Radial distribution functions relative to MeAcr$^+$ methyl carbon with Al atoms in dry Opt1 and Opt8 structures in Figure S2. The radial distribution functions, calculated from the room temperature trajectory MD1, relative to water with MeAcr$^+$ atoms are reported in Figure S3, and those relative to water−water are reported in Figure S4. Table S1, showing the experimental electronic transition energies and vibronic assignment for MeAcr$^+$ in water. Description of the ZL synthesis procedure. Movie 1 (mpeg file), showing MeAcr$^+$ mobility in a dry MeAcr$^+$−ZL system.

■ AUTHOR INFORMATION

Corresponding Author

*E-mail: fois@fis.unico.it.

Notes

The authors declare no competing financial interest.

■ ACKNOWLEDGMENTS

Financial support by Miur (Prin project 2010CX2TLM "InfoChem" and FIRB project RBFR12CLQD "ImPACT") is gratefully acknowledged. CINECA supercomputing center (Bologna, Italy) is gratefully acknowledged for computing time (ISCRA project "ZeoDye" HP10B8FNIH). A.D., P.B., and D.B. acknowledge financial support by the Swiss Commission for Technology and Innovation (KTI/CTI, Project 12902.1 PFNM-NM).

■ REFERENCES

(1) Calzaferri, G. *NANOCHANNELS.* Hosts for supramolecular organization of molecules and complexes. *Langmuir* **2012**, *28*, 6216−6231.

(2) Hashimoto, S. Optical Spectroscopy and Microscopy Studies on the Spatial Distribution and Reaction Dynamics in Zeolites. *J. Phys. Chem. Lett.* **2011**, *2*, 509−519.

(3) Cucinotta, F.; Popovic, Z.; Weiss, E. A.; Whitesides, G. M.; De Cola, L. Microcontact Transfer Printing of Zeolite Monolayers. *Adv. Mater.* **2009**, *21*, 1142−1145.

(4) Yoon, K. B. Organization of Zeolite Microcrystals for Production of Functional Materials. *Acc. Chem. Res.* **2007**, *40*, 29−40.
(5) Hashimoto, S.; Hagiri, M.; Matsubara, N.; Tobita, S. Photophysical studies of neutral aromatic species confined in zeolite L: Comparison with cationic dyes. *Phys. Chem. Chem. Phys.* **2001**, *3*, 5043−5051.
(6) Calzaferri, G.; Devaux, A. Manipulation of energy transfer processes within the channels of L-zeolite. In *SUPRAMOLECULAR PHOTOCHEMISTRY; Controlling Photochemical Processes*; Ramamurthy, V., Inoue, Y., Eds.; John Wiley & Sons: New York, 2011; Chapter 9, pp 285−387.
(7) International Zeolite Association, http://www.iza-structure.org.
(8) Ohsuna, T.; Slater, B.; Gao, F.; Yu, J.; Sakamoto, Y.; Zhu, G.; Terasaki, O.; Vaughan, D. E.; Qiu, S.; Catlow, C. R. Fine Structures of Zeolite-Linde-L (LTL): Surface Structures, Growth Unit and Defects. *Chem.—Eur. J.* **2004**, *10*, 5031−5040.
(9) Gaona-Gómez, A.; Cheng, C.-H. Modification of zeolite L (LTL) morphology using diols, $(OH)_2(CH_2)_{2n+2}O_n$ (n = 0,1, and 2). *Microporous Mesoporous Mater.* **2012**, *153*, 227−235.
(10) Zabala Ruiz, A.; Brühwiler, D.; Ban, T.; Calzaferri, G. Synthesis of Zeolite L. Tuning Size and Morphology. *Monatsh. Chem.* **2005**, *136*, 77−89.
(11) DeWilde, W.; Peeters, G.; Lunsford, J. H. Synthesis and Spectroscopic Properties of Tris(2,2′-bipyridine)ruthenium(II)in Zeolite Y. *J. Phys. Chem.* **1980**, *84*, 2306−2310.
(12) Cao, P.; Wang, Y.; Li, H.; Yu, X. Transparent, luminescent, and highly organized monolayers of zeolite L. *J. Mater. Chem.* **2011**, *21*, 2709−2714.
(13) Calzaferri, G.; Lutkouskaya, K. Mimicking the Antenna System of Green Plants. *Photochem. Photobiol. Sci.* **2008**, *7*, 879−910.
(14) Ramamurthy, V. *Photoprocesses of Organic Molecules Included in Zeolites in Photochemistry in Organized & Constrained Media*; VCH-Publishers: New York, 1991; Chapter 10, pp 429−493.
(15) Caro, J.; Marlow, F.; Wübbenhorst, M. Chromophore-Zeolite Composites: The Organizing Role of Molecular Sieves. *Adv. Mater.* **1994**, *6*, 413−416.
(16) Schulz-Ekloff, G.; Wöhrle, D.; van Duffel, B.; Schoonheydt, R. A. Chromophores in porous silicas and minerals: preparation and optical properties. *Microporous Mesoporous Mater.* **2002**, *51*, 91−138.
(17) Maggini, L.; Bonifazi, D. Hierarchised luminescent organic architectures: design, synthesis, self-assembly, self-organisation and functions. *Chem. Soc. Rev.* **2012**, *41*, 211−241.
(18) Huber, S.; Zabala Ruiz, A.; Li, H.; Patrinoiu, G.; Botta, Ch.; Calzaferri, G. Optical spectroscopy of inorganic-organic host-guest nanocrystals organized as oriented monolayers. *Inorg. Chim. Acta* **2007**, *360*, 869−875.
(19) Calzaferri, G.; Méallet-Renault, R.; Brühwiler, D.; Pansu, R.; Dolamic, I.; Dienel, T.; Adler, P.; Li, H.; Kunzmann, A. Designing Dye-Nanochannel Antenna Hybrid Materials for Light Harvesting, Transport and Trapping. *ChemPhysChem* **2011**, *12*, 580−594.
(20) Blum, C.; Cesa, Y.; Escalante, M.; Subramaniam, V. Multimode microscopy: spectral and lifetime imaging. *J. R. Soc. Interface* **2009**, *6*, S35−S43.
(21) Megelski, S.; Lieb, A.; Pauchard, M.; Drechsler, A.; Glaus, S.; Debus, C.; Meixner, A. J.; Calzaferri, G. Orientation of Fluorescent Dyes in the Nano Channels of Zeolite L. *J. Phys. Chem. B* **2001**, *105*, 25−35.
(22) Gasecka, A.; Dieu, L.-Q.; Brühwiler, D.; Brasselet, S. Probing Molecular Order in Zeolite L Inclusion Compounds Using Two-Photon Fluorescence Polarimetric Microscopy. *J. Phys. Chem. B* **2010**, *114*, 4192−4198.
(23) Nachtigal, P.; Sauer, J. Application of quantum chemical methods in zeolite science. In *Introduction to zeolite science and practice*, 3rd ed.; Cejka, J., van Bekkum, H., Corma, A., Schüth, F., Eds.; Elsevier: Amsterdam, 2007; Chapter 20, pp 701−736.
(24) Nusterer, R.; B1öchl, P. E.; Schwarz, K. Interaction of water and methanol with a zeolite at high coverages. *Chem. Phys. Lett.* **1996**, *253*, 448−455.
(25) Fois, E.; Tabacchi, G.; Calzaferri, G. Orientation and Order of Xanthene Dyes in the One-Dimensional Channels of Zeolite L: Bridging the Gap between Experimental Data and Molecular Behavior. *J. Phys. Chem. C* **2012**, *116*, 16784−16799.
(26) Fois, E.; Tabacchi, G.; Calzaferri, G. Interactions, behavior and stability of fluorenone inside zeolite nanochannels. *J. Phys. Chem. C* **2010**, *114*, 10572−10579.
(27) Zhou, X.; Wesolowski, T. A.; Tabacchi, G.; Fois, E.; Calzaferri, G.; Devaux, A. First-principles simulations of absorption bands of fluorenone in zeolite L. *Phys. Chem. Chem. Phys.* **2013**, *15*, 159−167.
(28) Matsuoka, Y.; Yamaoka, K. Film Dichroism. II. Linearly-polarized Absorption Spectra of Acridine Dyes in Streched Poly(vinyl alcohol) Films. *Bull. Chem. Soc. Jpn.* **1979**, *52*, 3163−3170.
(29) Matsuoka, Y. Film Dichroism. 4. Linear Dichroism Study of Orientation Behaviour of Planar Molecules in Streched Poly(vinyl alcohol) Film. *J. Phys. Chem.* **1980**, *84*, 1361−1366.
(30) Randic, M. Aromaticity of Polycyclic Conjugated Hydrocarbons. *Chem. Rev.* **2003**, *103*, 3449−3605.
(31) Lakowicz, J. R. *Principles of Fluorescence Spectroscopy*, 3rd ed.; Springer: Singapore, 2006.
(32) Calzaferri, G.; Brühwiler, D.; Megelski, S.; Pfenniger, M.; Pauchard, M.; Hennessy, B.; Maas, H.; Devaux, A.; Graf, U. Playing with Dye Molecules at the Inner and Outer Surface of Zeolite L. *Solid State Sci.* **2000**, *2*, 421−447.
(33) Hammond, P. R. Self-absorption of molecular fluorescence, the design of equipment for measurement of fluorescence decay, and the decay times of some laser dyes. *J. Chem. Phys.* **1979**, *70*, 3884−3894.
(34) Batchelder, J. S.; Zewail, A. H.; Cole, T. Luminescent solar concentrators. 1: Theory of operation and techniques for performance evaluation. *Appl. Opt.* **1979**, *18*, 3090−3110.
(35) Stanton, J. F.; Bartlett, R. J. Equation of motion coupled-cluster method: A systematic biorthogonal approach to molecular excitation energies, transition probabilities, and excited state properties. *J. Chem. Phys.* **1993**, *98*, 7029−7039.
(36) Yanai, T.; Tew, D.; Handy, N. A new hybrid exchange-correlation functional using the Coulomb-attenuating method (CAM-B3LYP). *Chem. Phys. Lett.* **2004**, *393*, 51−57.
(37) Casida, M. E.; Jamorski, C.; Casida, K. C.; Salahub, D. R. Molecular excitation energies to high-lying bound states from time-dependent density-functional response theory: Characterization and correction of the time-dependent local density approximation ionization threshold. *J. Chem. Phys.* **1998**, *108*, 4439−49.
(38) Fois, E.; Gamba, A.; Tabacchi, G.; Quartieri, S.; Vezzalini, G. Water molecules in single file: First-principles studies of one-dimensional water chains in zeolites. *J. Phys. Chem. B* **2001**, *105*, 3012−3016.
(39) Fois, E.; Gamba, A.; Tabacchi, G.; Quartieri, S.; Vezzalini, G. On the collective properties of water molecules in one-dimensional zeolitic channels. *Phys. Chem. Chem. Phys.* **2001**, *3*, 4158−4163.
(40) Pedone, A.; Bloino, J.; Barone, V. Role of Host-Guest interactions in tuning the optical properties of Coumarin derivatives in MCM-41: A TD-DFT investigation. *J. Phys. Chem. C* **2012**, *116*, 17807−17818.
(41) Tilocca, A.; Fois, E. The color and stability of Maya Blue: TDDFT calculations. *J. Phys. Chem. C* **2009**, *113*, 8683−8687.
(42) Giustetto, R.; Seenivasan, K.; Bonino, F.; Ricchiardi, G.; Bordiga, S.; Chierotti, M. R.; Gobetto, R. Host/Guest interactions in a Sepiolite-based Maya Blue Pigment: A spectroscopic Study. *J. Phys. Chem. C* **2013**, *115*, 16764−16776.
(43) Adeyemi, O. O.; Malinovskii, V. L.; Biner, S. A.; Calzaferri, G.; Häner, R. Photon harvesting by excimer-forming multichromophores. *Chem. Commun.* **2012**, *48*, 9589−9591.
(44) Wang, Y.; Li, H.; Feng, Y.; Zhang, H.; Calzaferri, G.; Ren, T. Orienting Zeolite L microcrystals with a functional linker. *Angew. Chem. Int. Ed.* **2010**, *49*, 1434−1438.
(45) Tomasi, J.; Mennucci, B.; Cammi, R. Quantum Mechanical Continuum Solvation Models. *Chem. Rev.* **2005**, *105*, 2999−3094.
(46) Hill, J. G. Gaussian basis sets for molecular applications. *Int. J. Quantum Chem.* **2013**, *113*, 21−34.

(47) Frisch, M. J.; Trucks, G. W.; Schlegel, H. B.; Scuseria, G. E.; Robb, M. A.; Cheeseman, J. R.; Scalmani, G.; Barone, V.; Mennucci, B.; Petersson, G. A.; Nakatsuji, H.; Caricato, M.; Li, X.; Hratchian, H. P.; Izmaylov, A. F.; Bloino, J.; Zheng, G.; Sonnenberg, J. L.; Hada, M.; Ehara, M.; Toyota, K.; Fukuda, R.; Hasegawa, J.; Ishida, M.; Nakajima, T.; Honda, Y.; Kitao, O.; Nakai, H.; Vreven, T.; Montgomery, Jr., J. A.; Peralta, J. E.; Ogliaro, F.; Bearpark, M.; Heyd, J. J.; Brothers, E.; Kudin, K. N.; Staroverov, V. N.; Kobayashi, R.; Normand, J.; Raghavachari, K.; Rendell, A.; Burant, J. C.; Iyengar, S. S.; Tomasi, J.; Cossi, M.; Rega, N.; Millam, J. M.; Klene, M.; Knox, J. E.; Cross, J. B.; Bakken, V.; Adamo, C.; Jaramillo, J.; Gomperts, R.; Stratmann, R. E.; Yazyev, O.; Austin, A. J.; Cammi, R.; Pomelli, C.; Ochterski, J. W.; Martin, R. L.; Morokuma, K.; Zakrzewski, V. G.; Voth, G. A.; Salvador, P.; Dannenberg, J. J.; Dapprich, S.; Daniels, A. D.; Farkas, Ö.; Foresman, J. B.; Ortiz, J. V.; Cioslowski, J.; Fox, D. J. *Gaussian 09*, revision B.01; Gaussian, Inc.: Wallingford, CT, 2009.

(48) Perdew, J. P.; Burke, K.; Ernzerhof, M. Generalized gradient approximation made simple. *Phys. Rev. Lett.* **1996**, *77*, 3865−3868.

(49) Newsam, J. M. Structures of dehydrated potassium zeolite-L at 298 and 78 K containing sorbed perdeuteriobenzene. *J. Phys. Chem.* **1989**, *93*, 7689−7694.

(50) Barrer, R. M.; Villiger, H. Z. The crystal structure of the synthetic zeolite L. *Kristallogr.* **1969**, *128*, 352−370.

(51) Vanderbilt, D. Soft self-consistent pseudopotentials in a generalized eigenvalue formalism. *Phys. Rev. B* **1990**, *41*, 7892−7895.

(52) Kleinman, K.; Bylander, D. M. Efficacious form for model pseudopotentials. *Phys. Rev. Lett.* **1982**, *48*, 1425−1428.

(53) Hamann, D. R.; Schlüter, M.; Chiang, C. Norm-conserving pseudopotentials. *Phys. Rev. Lett.* **1979**, *43*, 1494−1497.

(54) Troullier, N.; Martins, J. L. Efficient pseudopotentials for planewaves calculations. *Phys. Rev. B* **1991**, *43*, 1993−2006.

(55) Gamba, A.; Tabacchi, G.; Fois, E. TS-1 from First Principles. *J. Phys. Chem A* **2009**, *113*, 15006−15015.

(56) Fois, E.; Tabacchi, G.; Barreca, D.; Gasparotto, A.; Tondello, E. "Hot" Surface Activation of Molecular Complexes: Insight from Modeling Studies. *Angew. Chem., Int. Ed.* **2010**, *49*, 1944−1948.

(57) Car, R.; Parrinello, M. Unified approach for molecular dynamics and density functional theory. *Phys. Rev. Lett.* **1985**, *55*, 2471−2475.

(58) Marx, D.; Hutter, J. *Ab Initio Molecular Dynamics*; Cambridge University Press: New York, 2009.

(59) CPMD code, MPI für Festkörperforschung: Stuttgart, Germany; IBM Zürich Research Laboratory: Zürich, Switzerland, 1990−2012, www.cpmd.org.

(60) Nose, S. A unified formulation of the constant temperature molecular-dynamics methods. *J. Chem. Phys.* **1984**, *81*, 511−519.